INTERNATIONAL JOURNAL OF ROBUST AND NONLINEAR CONTROL
Int. J. Robust Nonlinear Control 2016; **26**:1162–1183
Published online 16 July 2015 in Wiley Online Library (wileyonlinelibrary.com). DOI: 10.1002/rnc.3386

Design of networked freeway traffic controllers based on event-triggered control concepts

Antonella Ferrara[1], Simona Sacone[2] and Silvia Siri[2,*,†]

[1]*Department of Electrical, Computer and Biomedical Engineering, University of Pavia, Italy*
[2]*Department of Informatics, Bioengineering, Robotics and Systems Engineering, University of Genova, Italy*

SUMMARY

In this paper, an event-triggered model predictive networked scheme is proposed to control traffic in freeway networks. The freeway network is a spatially distributed system in which sensors and actuators act locally on portions of the overall system; measurements and control actions are transmitted to/from the feedback controllers via a shared communication network. In this sense, the considered plant can be properly controlled by relying on a design framework typical of networked control systems, a major feature of which is the necessity of taking care of both the computational effort and the communication effort. The proposed control scheme allows to reduce the computational load with a feedback model predictive controller in which suitable triggering conditions are defined. As for the communication effort, local triggering conditions are included in sensors, inducing transmissions of the system state only when such conditions are verified. The robustness properties of the controlled system are investigated in the paper by analyzing the input-to-state practical stability of the plant under the action of the proposed control strategy. The effectiveness of this proposal is also analyzed via simulation. Copyright © 2015 John Wiley & Sons, Ltd.

Received 10 December 2014; Revised 21 May 2015; Accepted 31 May 2015

KEY WORDS: traffic control; event-triggered MPC; input-to-state stability

1. INTRODUCTION

Traffic congestion represents a critical problem for the daily life of many citizens all over the world. Congestion phenomena in urban and freeway networks can be solved not only by building new infrastructures, in order to increase road capacity, but also by properly adopting advanced technology and control systems. For this reason, the development of control techniques for freeway traffic systems has been a relevant research topic for several decades and still represents a challenging issue to be studied. Freeways can be controlled in different ways: the most widely used control action is ramp metering, which consists in regulating the flows of vehicles accessing the freeway using traffic lights located at the on-ramps [1]. Specifically, ramp metering is applied to achieve maximum mainstream throughput downstream of the ramp or, more generally, optimal freeway network traffic conditions [2].

One of the first effective ramp metering strategies is the local feedback traffic controller ALINEA [3], developed in the nineties, which has been applied in many freeways worldwide. Different traffic control methodologies have been developed in the last decades, also including approaches based on optimization or optimal control algorithms [4]. In some of these works, the problem of controlling a freeway is formulated as a discrete-time constrained nonlinear optimal control problem, whose numerical solution is often hard to find because of the problem dimensions and complexity. A very

*Correspondence to: Silvia Siri, Department of Informatics, Bioengineering, Robotics and Systems Engineering, University of Genova, Via Opera Pia 13, 16145, Genova, Italy.
†E-mail: silvia.siri@unige.it

efficient numerical solution algorithm has been adopted in the optimal freeway traffic control tool AMOC [5, 6], by using the so-called feasible direction algorithm. An alternative approach is the receding-horizon based model predictive control (MPC), which, in the specific application case, needs to be applied in real time. In the literature, MPC has been extensively adopted to control freeway traffic. For instance, in [7, 8], the nonlinear MPC framework is designed to include, as a predictor, the macroscopic model called METANET [9]. In other papers, for example [10, 11], the considered prediction model is instead the cell transmission model (CTM) [12, 13], suitably reformulated in mixed logical dynamical (MLD) form [14].

A major feature of freeway traffic control systems that has not yet received significant attention is the necessity of considering not only the controller of the plant but also all the measurement equipment (sensors) and the way in which all the system components are connected and communicate. When a plant is a spatially distributed system in which the communication between feedback controllers, sensors, and actuators occurs via a shared communication network, the control system is classified as a networked control system [15, 16].

In this paper, we propose a control framework aimed at reducing congestion in freeway systems considered as networked control systems, referring in particular to the cases in which the communication between the sensors and the controller occurs through a shared digital communication network. In the design of the control scheme, specific attention is devoted to reduce the communication effort. More specifically, the number of state transmissions between the sensors and the controller is decreased by defining specific sensor triggering conditions in order to evaluate whether the measurements obtained by sensors must be sent to the controller or not. Moreover, the proposed control scheme aims to reduce the computational effort, that is, the number of times in which the control law is computed. To this end, the controller proposed in this work, which implements an MPC strategy, is of event-triggered nature. The basic idea is that the control action is not computed at each sample time step (as in classical time-driven MPC schemes) but whenever suitable triggering conditions are satisfied, in analogy with [10] and [11].

The proposed control approach is theoretically analyzed in the paper, taking into account the fact that in a traffic control problem, the exogenous inputs can be estimated but are characterized by a significant level of uncertainty. For this reason, it is of paramount importance to adopt control strategies that prove to be able to maintain a good performance of the controlled system in the presence of uncertain exogenous signals. This feature is related to the robustness property of the controlled plant. A possibility could be that of adopting a robust predictive controller for freeway networks, as carried out in [17] where a min–max control scheme is proposed, explicitly including uncertainties in the control design phase. Yet, in the present work, we have preferred to use a control scheme not expressly designed to be robust and verify its natural robustness properties. This can be carried out by analyzing the input-to-state stability of the plant with respect to disturbances [18–20]. Specifically, in the paper, the input-to-state practical stability (ISpS) of the controlled system is proved.

The paper is organized as follows. Section 2 describes the proposed control framework for a general plant, whereas the event-triggered controller and the event-triggered sensors are specifically described for a freeway traffic system, respectively, in Section 3 and in Section 4. Section 5 is devoted to the analysis of the robustness features of the proposed event-triggered traffic control scheme. A detailed simulation campaign is discussed in Section 6, while some conclusive remarks are drawn in Section 7.

2. THE PROPOSED CONTROL FRAMEWORK

The proposed control framework is shown in Figure 1 for a general plant. The plant is composed of N subsystems, each of which is equipped with a sensor that measures the local state of the corresponding subsystem. The plant is regulated by a feedback controller, connected to measurement and actuation devices through a communication network.

As previously mentioned, this work is devoted to design a freeway traffic control scheme in which the computational and the communication efforts are minimized. Hence, both the controller and the sensors are characterized by the presence of event-triggered logics. In particular, the communication

DOI: 10.1002/rnc

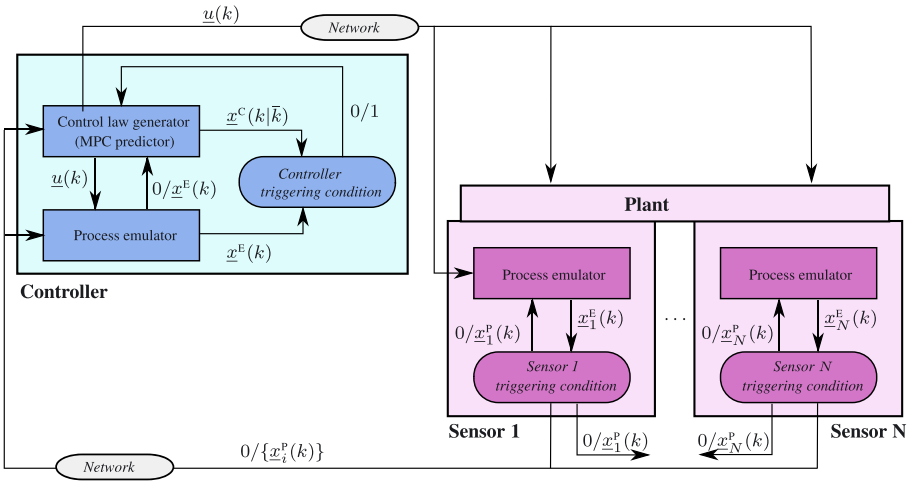

Figure 1. The proposed control scheme.

effort to be minimized regards the transmissions of the measurements of the system state from the sensors to the controller. Note that in this paper, it is supposed that it is not necessary to reduce the number of transmissions of the control action computed by the controller, this not being too heavy in practice because, generally, in freeway traffic, the number of control variables is definitely smaller than the number of state variables. If in field implementations this were not the case, solutions such as packetized MPC could be adopted [21].

Because the measurements are not transmitted at each time step, both the controller and the sensors are equipped with a process emulator that is able to reproduce the plant state dynamic evolution in a very accurate way. The reduction of the number of computations is achieved by computing the control law either when there is a significant deviation between the state predicted by the emulator and the one predicted by the control law generator or when new measurements are received from the plant. Moreover, state transmissions are limited to the cases in which there is a significant deviation between the real system state and the one predicted by the emulator. Because each subsystem is provided with a sensor that is able to measure the local plant state, at each time step, each sensor decides whether to send the measurement to the other sensors and to the controller, verifying if the difference between the measured state and the one provided by the emulator exceeds a given threshold.

Referring to a generic time step k, $\underline{u}(k)$ is the control action, whereas the system state is represented in three different ways: $\underline{x}^{\mathrm{C}}(k|\bar{k})$ is the state predicted by the control law generator according to the last solution computed at time step $\bar{k}$, $\underline{x}^{\mathrm{E}}(k)$ is the state predicted by the process emulator, and $\underline{x}^{\mathrm{P}}(k)$ is the real state of the plant. Because the plant is composed of N subsystems, let $\underline{x}_i^{\mathrm{P}}(k)$ denote the state of the plant referred to a generic subsystem i, measured by sensor i, $i = 1, \ldots, N$, and $\underline{x}_i^{\mathrm{E}}(k)$ denote the state of the plant subsystem i provided by the emulator. Note that the total plant state $\underline{x}^{\mathrm{P}}(k)$ is obtained by putting together the states $\underline{x}_i^{\mathrm{P}}(k)$ measured in each subsystem $i = 1, \ldots, N$, and obviously, the same holds for the system predicted by the emulator. Moreover, let $\mathcal{I}(k) \subseteq \{1 \ldots, N\}$ indicate the set of sensors that transmit their measurements at time step k.

Let us now describe in detail each block of the proposed scheme. First of all, the designed controller is of event-triggered predictive type and is made of three blocks.

- The *control law generator* is a model predictive controller that computes the control law by solving a finite-horizon optimal control problem in which a system prediction model is considered among the constraints. Such a problem is not solved at each time step but only when the control law generator is activated either by the controller triggering condition or by a new transmission of the system state. If the control law generator is activated by the controller triggering condition, the controller uses as initial conditions the state $\underline{x}^{\mathrm{E}}(k)$ generated by the emulator. If instead the control law generator is activated by the transmission of new

DOI: 10.1002/rnc

measurements $\underline{x}_i^{\mathrm{P}}(k)$, $i \in \mathcal{I}(k)$, the initial condition of the controller is updated so as to include the received $\underline{x}_i^{\mathrm{P}}(k)$, $i \in \mathcal{I}(k)$. At each time step k, supposing that the control law has been computed at time step $\bar{k} < k$, the control law generator provides the predicted state $\underline{x}^{\mathrm{C}}(k|\bar{k})$ and the control $\underline{u}(k) = \underline{u}^{\mathrm{C}}(k|\bar{k})$.

- The *process emulator* provides a prediction of the system state by using a model of its dynamic behavior. The model adopted in the process emulator is, in general, more detailed than the prediction model adopted in the MPC scheme. By receiving at each time step k the control action $\underline{u}(k)$ computed by the control law generator, the process emulator is able to reproduce the behavior of the real system by generating the state $\underline{x}^{\mathrm{E}}(k)$; the emulator updates this state when it receives new measurements of the real state of the plant $\underline{x}_i^{\mathrm{P}}(k)$, $i \in \mathcal{I}(k)$.
- The *controller triggering condition* is used to determine if the control law must be generated again, that is, a new finite-horizon optimal control problem must be solved, or if the control law already computed is still suitable to be applied to the real system. At each time step k, on the basis of the state $\underline{x}^{\mathrm{C}}(k|\bar{k})$ predicted by the controller and the state $\underline{x}^{\mathrm{E}}(k)$ generated by the process emulator, the triggering condition is checked, and a binary triggering signal is communicated to the control law generator.

The plant, and specifically all the actuators, receives at each time step k the control $\underline{u}(k)$ to be applied. The real state of each plant subsystem $\underline{x}_i^{\mathrm{P}}(k)$ is measured by sensor i at each time step k, but it is transmitted only when this is considered useful to guarantee good performances of the controlled freeway system. In particular, referring again to Figure 1, each sensor i, $i = 1, \ldots, N$, can be represented with two blocks.

- The *process emulator* is the same used in the controller. At time step k, it receives the control $\underline{u}(k)$ and generates the state $\underline{x}^{\mathrm{E}}(k)$. All the process emulators (in the sensors and in the controller) are completely synchronized because they use the same model, update the state simultaneously, and consider the same control $\underline{u}(k)$.
- The *sensor triggering condition* compares the state $\underline{x}_i^{\mathrm{E}}(k)$ provided by the emulator and referred to subsystem i with the measured state $\underline{x}_i^{\mathrm{P}}(k)$. Only if such a difference is greater than a given threshold, the measured state is transmitted to the controller and to the other sensors. In this way, this measurement is used as initial state for the control law generator and for all the process emulators, in the sensors and in the controller.

3. THE EVENT-TRIGGERED CONTROLLER IN A FREEWAY TRAFFIC SYSTEM

The controller adopted in the proposed control framework can be classified as an event-triggered MPC. The control law generator, the process emulator, and the controller triggering conditions will be customized in this section with reference to the freeway traffic control case.

In the considered traffic control scheme, a subdivision of the freeway into cells and a discretization of the time horizon are made. Let N be the number of cells, K the number of time steps, T the sample time, and L_i the length of cell i, $i = 1, \ldots, N$. The space and time discretizations are the same for the control law generator, the process emulators, and the plant model.

3.1. The control law generator

The control law generator applies an MPC scheme, which determines the control action to be applied to the freeway system. In this paper, ramp metering is applied; that is, the control variables are the flows entering the freeway from on-ramps.

The prediction model used in the finite-horizon optimal control problem is the first-order macroscopic traffic model known as CTM [12, 13]. Let us define the following quantities referred to a generic time step k (see Figure 2):

- $\rho_i(k)$ traffic density of cell i [veh/km];
- $\phi_i(k)$ mainstream flow entering cell i from cell $i-1$ [veh/h];
- $l_i(k)$ queue length in the on-ramp of cell i [veh];
- $r_i(k)$ flow entering cell i from the on-ramp [veh/h];

DOI: 10.1002/rnc

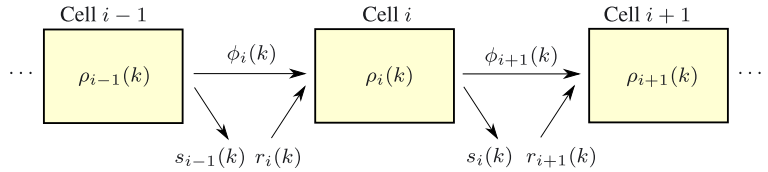

Figure 2. Sketch of the subdivision of the freeway into cells.

- $d_i(k)$ on-ramp demand referred to cell i [veh/h];
- $s_i(k)$ flow exiting cell i through the off-ramp [veh/h];
- $D_i(k)$ demand, $S_i(k)$ supply of cell i [veh/h].

The CTM parameters are: $\beta_i \in [0, 1)$ split ratio, F_i capacity [veh/h], $\bar{\rho}_i$ jam density [veh/km], w_i congestion wave speed [km/h], v_i free flow speed [km/h], and $p_i \in [0, 1]$ priority of the on-ramp flow with respect to the mainstream flow of cell i.

The dynamic model is given by the state equations for the traffic density $\rho_i(k)$ and the queue length $l_i(k)$, $i = 1, \ldots, N$, $k = 1, \ldots, K$, that is,

$$\rho_i(k+1) = \rho_i(k) + \frac{T}{L_i}\left[\phi_i(k) + r_i(k) - \phi_{i+1}(k) - s_i(k)\right] \tag{1}$$

$$l_i(k+1) = l_i(k) + T\left[d_i(k) - r_i(k)\right] \tag{2}$$

where $s_i(k) = \frac{\beta_i}{1-\beta_i}\phi_{i+1}(k)$. Referring to cell i, it is useful to define the demand of cell $i-1$ and the supply of cell i as follows:

$$D_{i-1}(k) = \min\left\{(1-\beta_{i-1})v_{i-1}\rho_{i-1}(k), F_{i-1}\right\} \tag{3}$$

$$S_i(k) = \min\left\{w_i(\bar{\rho}_i - \rho_i(k)), F_i\right\} \tag{4}$$

The mainstream and on-ramp flows are obtained as

$$\begin{aligned}
&\text{If} \quad D_{i-1}(k) + d_i(k) + \frac{l_i(k)}{T} \leqslant S_i(k)\\
&\text{then}\\
&\phi_i(k) = D_{i-1}(k), \quad r_i(k) = d_i(k) + \frac{l_i(k)}{T}\\
&\text{else}\\
&\phi_i(k) = \text{mid}\left\{D_{i-1}(k), S_i(k) - d_i(k) - \frac{l_i(k)}{T}, (1-p_i)S_i(k)\right\}\\
&r_i(k) = \text{mid}\left\{d_i(k) + \frac{l_i(k)}{T}, S_i(k) - D_{i-1}(k), p_i S_i(k)\right\}
\end{aligned} \tag{5}$$

where the function mid returns the middle value.

Because the previous equations include nonlinearities (due to min and mid functions in (3), (4), and (5)), the CTM has been properly rewritten in MLD form, by introducing some sets of inequalities and auxiliary variables, in order to obtain a mixed-integer linear model. For space limitations, we do not report all the inequalities and the auxiliary variables of the MLD formulation (the interested reader can find more details on the CTM in MLD form in [11]). In this reformulation of the CTM, three sets of binary auxiliary variables and five sets of real auxiliary variables are defined; let us denote them, respectively, as $\delta_{i,j}(k)$, $j = 1, \ldots, 3$, and $z_{i,j}(k)$, $j = 1, \ldots, 5$, $i = 1, \ldots, N$, $k = 1, \ldots, K$.

The adopted objective function is defined as the weighted sum of traffic densities, queue lengths, and terms penalizing the cases in which the traffic density exceeds a given threshold value. The

DOI: 10.1002/rnc

threshold values for the traffic density are denoted as ρ_i^{t}, $i = 1, \ldots, N$. Then, it is necessary to introduce a set of variables $\varrho_i(k)$, $i = 1, \ldots, N$, $k = 1, \ldots, K$, defined as follows:

$$\varrho_i(k) = \begin{cases} \rho_i(k) - \rho_i^{\mathrm{t}} & \text{if } \rho_i(k) \geqslant \rho_i^{\mathrm{t}} \\ 0 & \text{otherwise} \end{cases} \tag{6}$$

The finite-horizon optimal control problem to be solved at time step k over a prediction horizon K_p is the following.

Problem 1
Given the initial conditions on the density and the queue lengths $\rho_i(k)$ and $l_i(k)$, $i = 1, \ldots, N$, the demand of the cell before the first one $D_0(h)$, $h = k, \ldots, k + K_p - 1$, the supply of the cell after the last one $S_{N+1}(h)$, $h = k, \ldots, k + K_p - 1$, and the on-ramp demands $d_i(h)$, $i = 1, \ldots, N$, $h = k, \ldots, k + K_p - 1$, find the optimal control variables $r_i(h)$, $i = 1, \ldots, N$, $h = k, \ldots, k + K_p - 1$, minimizing the cost function

$$J(k) = \sum_{h=k}^{k+K_p-1} \sum_{i=1}^{N} \gamma_i^{\rho} \rho_i(h) + \gamma_i^{l} l_i(h) + \gamma_i^{\varrho} \varrho_i(h) \tag{7}$$

subject to the CTM model in MLD form and

$$\varrho_i(h) \geqslant \rho_i(h) - \rho_i^{\mathrm{t}} \quad i = 1, \ldots, N, \ h = k+1, \ldots, k+K_p \tag{8}$$

$$\varrho_i(h) \geqslant 0 \qquad i = 1, \ldots, N, \ h = k+1, \ldots, k+K_p \tag{9}$$

$$0 \leqslant \rho_i(h) \leqslant \bar{\rho}_i \qquad i = 1, \ldots, N, \ h = k+1, \ldots, k+K_p \tag{10}$$

$$0 \leqslant l_i(h) \leqslant \bar{l}_i \qquad i = 1, \ldots, N, \ h = k+1, \ldots, k+K_p \tag{11}$$

$$0 \leqslant r_i(h) \leqslant \bar{r}_i \qquad i = 1, \ldots, N, \ h = k, \ldots, k+K_p-1 \tag{12}$$

■

In Problem 1, $\bar{l}_i$ and $\bar{r}_i$, $i = 1, \ldots, N$, represent the maximum values of queue lengths and on-ramp flows, respectively. Note that if $\gamma_i^{\rho} = TL_i$, $\gamma_i^{l} = T$, and $\gamma_i^{\varrho} = 0$, cost function (7) is the total time spent by vehicles in the network, which is an objective function commonly used in traffic control.

Problem 1 is a mixed-integer linear programming problem for which existing commercial solvers are able to find the optimal solution. Let us denote with $v^{\mathrm{C}}(h|k)$ the value of a generic quantity v referred to time step h, obtained as optimal solution of the finite-horizon problem solved at time step k. In particular, when Problem 1 is solved at time step k, the optimal control and state variables for the entire prediction horizon are obtained, that is, $r_i^{\mathrm{C}}(h|k)$, $i = 1, \ldots, N$, $h = k, \ldots, k + K_p - 1$ and $\rho_i^{\mathrm{C}}(h|k)$, $l_i^{\mathrm{C}}(h|k)$ $i = 1, \ldots, N$, $h = k, \ldots, k + K_p$. Let X_0 be the set of initial states $\rho_i(k)$ and $l_i(k)$, $i = 1, \ldots, N$, for which Problem 1 admits a feasible solution.

3.2. The process emulator

The process emulator can adopt, as dynamic model of the traffic behavior, either the CTM or more detailed traffic models, such as the second-order model METANET, and simple microscopic simulation models of the traffic dynamics [22, 23]. In any case, according to the notation introduced in Section 2, at time step k, the process emulator determines the state variables $\rho_i^{\mathrm{E}}(k)$ and $l_i^{\mathrm{E}}(k)$, $i = 1, \ldots, N$, which are gathered in the system state vector $\underline{x}^{\mathrm{E}}(k)$.

We suppose that the model used by the process emulator is very accurate in representing the plant dynamic behavior, which differs from the behavior provided by the emulator for some exogenous inputs. In other words, the system state given by the emulator can be considered as the nominal

DOI: 10.1002/rnc

system, whereas the plant can be regarded as the perturbed system. Hence, the system dynamics of the emulator in a general case can be written as

$$\underline{x}^{\mathrm{E}}(k+1) = f\left(\underline{x}^{\mathrm{E}}(k), \underline{u}(k)\right) \tag{13}$$

whereas the plant state (including the state variables $\rho_i^{\mathrm{P}}(k)$ and $l_i^{\mathrm{P}}(k)$, $i = 1, \ldots, N$) is assumed to evolve according to the following:

$$\underline{x}^{\mathrm{P}}(k+1) = f\left(\underline{x}^{\mathrm{P}}(k), \underline{u}(k)\right) + \underline{\omega}(k) \tag{14}$$

where $\underline{\omega}(k) \in W$ represents the possible exogenous inputs, for instance, external disturbances. The exogenous inputs are additive and bounded signals and $\|\underline{\omega}(k)\| \leqslant \Omega$, $\forall\, k$. Specifically, Ω_i^{ρ} and Ω_i^{l} are the maximum values of exogenous inputs affecting the traffic density and the on-ramp queue length in cell i, $i = 1, \ldots, N$. The assumption of additive and bounded exogenous inputs is made because the most important exogenous inputs in freeway traffic systems are the deviations between the real values of the traffic demands (on-ramp demands and demand of the cell before the first one) and their estimates. These terms are bounded and affect the evolution of the system state as additive contributions.

Note that if at time step k some measurements of the plant state $\rho_i^{\mathrm{P}}(k)$, $l_i^{\mathrm{P}}(k)$, $i \in \mathcal{I}(k)$, are sent to the controller, the emulator updates its state and, in particular, the part of the state relative to the cells that have transmitted the measurements, that is, $\rho_i^{\mathrm{E}}(k) = \rho_i^{\mathrm{P}}(k)$ and $l_i^{\mathrm{E}}(k) = l_i^{\mathrm{P}}(k)$, $i \in \mathcal{I}(k)$.

3.3. Controller triggering conditions

According to event-triggered control logics, the finite-horizon optimal control problem is not solved at each time step but only when a given set of conditions is satisfied. Let us call such a set of conditions *triggering rule* and the time steps in which the triggering rule is verified *triggering time steps*. As aforementioned, the triggering rule is verified when the controller triggering conditions are satisfied or when a new measurement is received from sensors.

The basic idea for the controller triggering conditions is that they are fulfilled when there is a significant difference between the predicted system state and the system state obtained by the process emulator. In fact, the errors between these two states give an indication about the effectiveness of the prediction in the finite-horizon optimal control problem and, consequently, of the control variables found. Of course, the controller triggering condition must verify also that $k - \bar{k} < K_p$; otherwise, the control sequence found in $\bar{k}$ is no more applicable.

Hence, considering that $\bar{k}$ is the previous triggering time step, the controller triggering conditions to be verified at a generic time step $k \geqslant \bar{k}$ can be written as

$$\exists i \in \{1, \ldots, N\} : \left|\rho_i^{\mathrm{E}}(k) - \rho_i^{\mathrm{C}}(k|\bar{k})\right| > \epsilon_i^{\rho} \tag{15}$$

$$\vee$$

$$\exists i \in \{1, \ldots, N\} : \left|l_i^{\mathrm{E}}(k) - l_i^{\mathrm{C}}(k|\bar{k})\right| > \epsilon_i^{l} \tag{16}$$

$$\vee$$

$$k \geqslant \bar{k} + K_p \tag{17}$$

where ϵ_i^{ρ} and ϵ_i^{l} are threshold values on the density and queue length errors, respectively, for cell i, $i = 1, \ldots, N$. Then, the overall triggering rule that activates the solution of a new finite-horizon optimal control problem is given by the controller triggering conditions (15), (16), and (17) and the check if a new measurement is received from sensors, that is,

$$\exists i \in \{1, \ldots, N\} : \rho_i^{\mathrm{P}}(k) \text{ is received from sensors} \tag{18}$$

$$\vee$$

$$\exists i \in \{1, \ldots, N\} : l_i^{\mathrm{P}}(k) \text{ is received from sensors} \tag{19}$$

The control strategy can be defined as follows. At $k = 0$, Problem 1 is solved determining the optimal control variables $r_i^{\mathrm{C}}(h|0)$, $i = 1, \ldots, N$, $h = 0, \ldots, K_p - 1$, and $r_i^{\mathrm{C}}(0|0)$ is applied. At each time step $k > 0$, the triggering rule is verified:

DOI: 10.1002/rnc

- if it is not met, the already-available control sequence is applied, that is, $r_i^{\mathrm{C}}(k|\bar{k})$ where $\bar{k}$ is the time step in which Problem 1 has been solved for the last time;
- if it is met, time step k becomes a triggering time step, Problem 1 is solved, the optimal control variables $r_i^{\mathrm{C}}(h|k)$, $i = 1, \ldots, N$, $h = k, \ldots, k + K_p - 1$ are derived, and $r_i^{\mathrm{C}}(k|k)$ is applied. Note that if the triggering rule is met because triggering conditions (15), (16), and (17) are verified, Problem 1 is solved by using as initial state the one provided by the emulator, that is, $\rho_i^{\mathrm{C}}(k|k) = \rho_i^{\mathrm{E}}(k)$ and $l_i^{\mathrm{C}}(k|k) = l_i^{\mathrm{E}}(k)$, $i = 1, \ldots, N$. If conditions (18) and (19) are verified, the initial state for Problem 1 is given by $\rho_i^{\mathrm{C}}(k|k) = \rho_i^{\mathrm{P}}(k)$ and $l_i^{\mathrm{C}}(k|k) = l_i^{\mathrm{P}}(k)$ for cells $i \in \mathcal{I}(k)$ and $\rho_i^{\mathrm{C}}(k|k) = \rho_i^{\mathrm{E}}(k)$ and $l_i^{\mathrm{C}}(k|k) = l_i^{\mathrm{E}}(k)$ for cells $i \notin \mathcal{I}(k)$.

Let us gather the triggering time steps in set $\Upsilon = \{k_c\}$, with $k_0 = 0$, $k_{c+1} > k_c$ and $k_{c+1} - k_c \leqslant K_p$.

4. THE EVENT-TRIGGERED SENSORS IN A FREEWAY TRAFFIC SYSTEM

In the present work, the sensors are smart in the sense that they not only measure the local system state but also decide when it must be transmitted to the controller. For simplicity, we suppose that sensors are capable of providing measurements of densities and on-ramp queue lengths along the freeway and that each cell is provided with a sensor. Apart from the measurement devices, sensors are composed of a process emulator and of a module devoted to trigger a new transmission.

4.1. The process emulator

As already mentioned, the process emulator in each sensor provides the system state variables $\rho_i^{\mathrm{E}}(k)$ and $l_i^{\mathrm{E}}(k)$, $i = 1, \ldots, N$, generated by the same process emulator present in the controller (described in Section 3.2). Analogously to the process emulator in the controller, the process emulators in the sensors update their state when a new transmission is received.

4.2. The sensor triggering condition

The objective of the sensor triggering condition is to transmit the measured system state and to activate the computation of the control law only when it is actually necessary. Then, whenever the system state determined by the process emulator in each sensor i, $i = 1, \ldots, N$, and the measured system state differ significantly, the system state is transmitted (to the controller and to the other sensors), the process emulators (in the controller and in the other sensors) update the system state, and a new computation of the control law is forced. Examples of triggering conditions applied in a different scheme can be found in [24].

More precisely, at a generic time step k, the sensor present in cell i, $i = 1, \ldots, N$, verifies the following triggering condition:

$$|\rho_i^{\mathrm{P}}(k) - \rho_i^{\mathrm{E}}(k)| > \kappa_i^{\rho}(k) \cdot \Omega_i^{\rho} \tag{20}$$

$$\vee$$

$$|l_i^{\mathrm{P}}(k) - l_i^{\mathrm{E}}(k)| > \kappa_i^{l}(k) \cdot \Omega_i^{l} \tag{21}$$

where $\kappa_i^{\rho}(k)$, $\kappa_i^{l}(k)$ are given threshold values. In case this condition is fulfilled, the sensor of cell i transmits the current measurement $\rho_i^{\mathrm{P}}(k)$ and $l_i^{\mathrm{P}}(k)$ to the controller and to all the other sensors (so that all the process emulators are updated synchronously).

5. ANALYSIS OF THE PROPOSED EVENT-TRIGGERED CONTROL SCHEME

Objective of this section is to study the robustness properties of the freeway system controlled via the proposed event-triggered MPC scheme. In particular, we are interested in analyzing the ISpS property of the controlled freeway system. Let us first of all introduce some classes of functions that will be used in the following results.

DOI: 10.1002/rnc

A function $f : \mathbb{R}^+ \to \mathbb{R}^+$ is a $\mathcal{K}$-function if it is continuous, strictly increasing, and $f(0) = 0$. A function $f : \mathbb{R}^+ \to \mathbb{R}^+$ is a $\mathcal{K}_\infty$-function if it is a $\mathcal{K}$-function and it is unbounded. A function $f : \mathbb{R}^+ \to \mathbb{R}^+$ is an $\mathcal{L}$-function if it is continuous, strictly decreasing, and $\lim_{\tau\to\infty} f(\tau) = 0$. A function $f : \mathbb{R}^+ \times \mathbb{R}^+ \to \mathbb{R}^+$ is a $\mathcal{KL}$-function if $f(\cdot, t)$ is a $\mathcal{K}$-function $\forall\, t \in \mathbb{R}^+$ and $f(s, \cdot)$ is an $\mathcal{L}$-function $\forall\, s \in \mathbb{R}^+$.

Moreover, let us recall some other useful definitions based on [18, 19, 25, 26].

Definition 1
Consider a system described by

$$\underline{x}(k+1) = \varphi(\underline{x}(k), \underline{\omega}(k)) \tag{22}$$

where $\underline{x}(k) \in X \subset \mathbb{R}^n$ is the system state and $\underline{\omega}(k) \in W$ is an exogenous input such that $\|\underline{\omega}(k)\| \leqslant \Omega$, $\forall\, k$. Considering a subset $X_{in} \subseteq X$, the system is input-to-state practically stable for initial conditions in X_{in} and exogenous inputs in W, if there exist a $\mathcal{KL}$ function $\beta(\cdot,\cdot)$, a $\mathcal{K}$-function $\gamma(\cdot)$, and a non-negative constant c such that

$$\|\underline{x}(k)\| \leqslant \beta(\|\underline{x}(0)\|, k) + \gamma(\Omega) + c, \quad \forall\, \underline{x}(0) \in X_{in}, \forall\, k \tag{23}$$

■

Definition 2
A continuous function $V(\cdot) : \mathbb{R}^n \longrightarrow \mathbb{R}^+$ is an ISpS Lyapunov function for system (22) with respect to initial conditions in X_{in} and exogenous inputs in W, if there exist $\mathcal{K}_\infty$-functions $\alpha_1(\cdot), \alpha_2(\cdot)$ and $\alpha_3(\cdot)$, a $\mathcal{K}$-function $\sigma(\cdot)$, and non-negative constants c_1 and c_2 such that for each state trajectory generated from $\underline{x}(0) \in X_{in}$,

$$\alpha_1(\|\underline{x}(k)\|) \leqslant V(\underline{x}(k)) \leqslant \alpha_2(\|\underline{x}(k)\|) + c_1, \quad \forall\, k \tag{24}$$

$$V(\varphi(\underline{x}(k), \underline{\omega}(k))) - V(\underline{x}(k)) \leqslant -\alpha_3(\|\underline{x}(k)\|) + \sigma(\|\underline{\omega}(k)\|) + c_2, \quad \forall\, \underline{\omega}(k) \in W, \forall\, k \tag{25}$$

■

Let us now introduce the following result that relates the plant state with the state predicted by the control law generator in a time interval between two consecutive triggering time steps.

Proposition 1
Consider a generic triggering time step $k_c \in \Upsilon$; by applying the control sequence $r_i^{\mathrm{C}}(h|k_c)$, $i = 1, \ldots, N$, $h = k_c, \ldots, k_{c+1} - 1$, to the plant, it holds:

$$\left|\rho_i^{\mathrm{P}}(h) - \rho_i^{\mathrm{C}}(h|k_c)\right| \leqslant \epsilon_i^{\rho} + \kappa_i^{\rho}(h) \cdot \Omega_i^{\rho} \qquad i = 1, \ldots, N,\ h = k_c + 1, \ldots, k_{c+1} - 1 \tag{26}$$

$$\left|l_i^{\mathrm{P}}(h) - l_i^{\mathrm{C}}(h|k_c)\right| \leqslant \epsilon_i^{l} + \kappa_i^{l}(h) \cdot \Omega_i^{l} \qquad i = 1, \ldots, N,\ h = k_c + 1, \ldots, k_{c+1} - 1 \tag{27}$$

Proof
Let us start by proving (26). It holds

$$\left|\rho_i^{\mathrm{P}}(h) - \rho_i^{\mathrm{C}}(h|k_c)\right| = \left|\rho_i^{\mathrm{P}}(h) - \rho_i^{\mathrm{E}}(h) + \rho_i^{\mathrm{E}}(h) - \rho_i^{\mathrm{C}}(h|k_c)\right| \leqslant |\rho_i^{\mathrm{P}}(h) - \rho_i^{\mathrm{E}}(h)| + \left|\rho_i^{\mathrm{E}}(h) - \rho_i^{\mathrm{C}}(h|k_c)\right| \tag{28}$$

DOI: 10.1002/rnc

Because in time steps $h = k_c + 1, \ldots, k_{c+1} - 1$ the control law is not updated, the triggering rule is not fulfilled. This means that (15) and (20) do not hold. Then

$$|\rho_i^{\mathrm{P}}(h) - \rho_i^{\mathrm{E}}(h)| + \left|\rho_i^{\mathrm{E}}(h) - \rho_i^{\mathrm{C}}(h|k_c)\right| \leqslant \kappa_i^{\rho}(h) \cdot \Omega_i^{\rho} + \epsilon_i^{\rho} \tag{29}$$

Similarly, to prove (27), it must be considered that in time steps $h = k_c + 1, \ldots, k_{c+1} - 1$, conditions (16) and (21) do not hold. Then it is possible to write

$$\left|l_i^{\mathrm{P}}(h) - l_i^{\mathrm{C}}(h|k_c)\right| \leqslant |l_i^{\mathrm{P}}(h) - l_i^{\mathrm{E}}(h)| + \left|l_i^{\mathrm{E}}(h) - l_i^{\mathrm{C}}(h|k_c)\right| \leqslant \kappa_i^{l}(h) \cdot \Omega_i^{l} + \epsilon_i^{l} \tag{30}$$

□

The following results consider the optimal value of the cost function (7) as a candidate ISpS Lyapunov function for which the necessary conditions are analyzed. In particular, the following two lemmas prove (24) and (25) for each triggering time step $k_c \in \Upsilon$.

Lemma 1
Consider a generic triggering time step $k_c \in \Upsilon$; it holds

$$\alpha_1(\|\underline{x}^{\mathrm{C}}(k_c|k_c)\|) \leqslant V(\underline{x}^{\mathrm{C}}(k_c|k_c)) \leqslant \alpha_2(\|\underline{x}^{\mathrm{C}}(k_c|k_c)\|) + c_1 \tag{31}$$

where $V(\cdot)$ is the value of the optimal cost function (7), $\alpha_1(\cdot)$ and $\alpha_2(\cdot)$ are $\mathcal{K}_\infty$-functions, and c_1 is a non-negative constant.

Proof
Because

$$V(\underline{x}^{\mathrm{C}}(k_c|k_c)) = \sum_{h=k_c}^{k_c+K_p-1} \sum_{i=1}^{N} \gamma_i^{\rho} \rho_i^{\mathrm{C}}(h|k_c) + \gamma_i^{l} l_i^{\mathrm{C}}(h|k_c) + \gamma_i^{\varrho} \varrho_i^{\mathrm{C}}(h|k_c) \tag{32}$$

considering $\gamma_i^{\min} = \min\{\gamma_i^{\rho}, \gamma_i^{l}, \gamma_i^{\varrho}\}$, $i = 1, \ldots, N$, $\gamma^{\min} = \min_i\{\gamma_i^{\min}\}$, $\gamma_i^{\max} = \max\{\gamma_i^{\rho} + \gamma_i^{\varrho}, \gamma_i^{l}\}$, $i = 1, \ldots, N$, $\gamma^{\max} = \max_i\{\gamma_i^{\max}\}$ and thanks to the nonnegativity of $\rho_i^{\mathrm{C}}(k), l_i^{\mathrm{C}}(k), i = 1, \ldots, N$, $k = 1, \ldots, K$, it holds

$$\begin{aligned} &\gamma^{\min} \sum_{i=1}^{N} \left|\rho_i^{\mathrm{C}}(k_c|k_c)\right| + \left|l_i^{\mathrm{C}}(k_c|k_c)\right| \leqslant V(\underline{x}^{\mathrm{C}}(k_c|k_c)) \\ &\leqslant \gamma^{\max} \sum_{i=1}^{N} \left|\rho_i^{\mathrm{C}}(k_c|k_c)\right| + \left|l_i^{\mathrm{C}}(k_c|k_c)\right| + \gamma^{\max}(K_p - 1) \sum_{i=1}^{N} \left(\bar{\rho}_i + \bar{l}_i\right) \end{aligned} \tag{33}$$

which proves (31) by considering the one-norm of the state variables. □

Lemma 2
Consider a generic triggering time step $k_c \in \Upsilon$; it holds

$$V(\underline{x}^{\mathrm{C}}(k_c + j\,|k_c + j)) - V(\underline{x}^{\mathrm{C}}(k_c|k_c)) \leqslant -\alpha_3(\|\underline{x}^{\mathrm{C}}(k_c|k_c)\|) + \sigma(\Omega) + c_2 \qquad j = 1, \ldots, k_{c+1} - k_c - 1 \tag{34}$$

where $V(\cdot)$ is the value of the optimal cost function (7), $\alpha_3(\cdot)$ is a $\mathcal{K}_\infty$-function, $\sigma(\cdot)$ is a $\mathcal{K}$-function, and c_2 is a non-negative constant.

Proof

Let us suppose to solve the finite-horizon optimal control problem at time step k_c and to determine $\underline{u}^{\mathrm{C}}(k_c + h|k_c)$, $h = 0, \ldots, K_p - 1$. Then, let us define a control sequence $\underline{\tilde{u}}(k_c + j + h)$, $h = 0, \ldots, K_p - 1$, with $\underline{\tilde{u}}(k_c + j + h) = \underline{u}^{\mathrm{C}}(k_c + j + h|k_c)$, $h = 0, \ldots, K_p - 1 - j$, and $\underline{\tilde{u}}(k_c + j + h) =$

DOI: 10.1002/rnc

$\underline{u}_{\text{aux}}(k_c+j+h)$, $h=K_p-j,\ldots,K_p-1$, $\underline{u}_{\text{aux}}(\cdot)$ being a feasible control action. Let us denote with $\mathcal{J}^{\text{P}}(\underline{x}^{\text{P}}(k_c+j))$ the cost function obtained starting from $\underline{x}^{\text{P}}(k_c+j)$ and applying the control sequence $\tilde{\underline{u}}(k_c+j+h)$, $h=0,\ldots,K_p-1$ to the plant. In particular, let $\rho_i^{\text{P}}(k_c+j+h)$, $l_j^{\text{P}}(k_c+j+h)$, $\varrho_i^{\text{P}}(k_c+j+h)$, $i=1,\ldots,N$, $h=0,\ldots,K_p-1-j$ and $\tilde{\rho}_i^{\text{P}}(k_c+j+h)$, $\tilde{l}_i^{\text{P}}(k_c+j+h)$, $\tilde{\varrho}_i^{\text{P}}(k_c+j+h)$, $i=1,\ldots,N$, $h=K_p-j,\ldots,K_p-1$, denote the corresponding variables obtained by applying the control sequence $\tilde{\underline{u}}(k_c+j+h)$, $h=0,\ldots,K_p-1$. Moreover, let us denote with $V(\underline{x}^{\text{C}}(k_c+j\,|k_c+j))$ the value of the optimal cost function that would be obtained if a finite-horizon optimal control problem were solved at time step k_c+j, $j=1,\ldots,k_{c+1}-k_c-1$.

The following holds:

$$V(\underline{x}^{\text{C}}(k_c+j\,|k_c+j))-V(\underline{x}^{\text{C}}(k_c|k_c))\leqslant\mathcal{J}^{\text{P}}(\underline{x}^{\text{P}}(k_c+j))-V(\underline{x}^{\text{C}}(k_c|k_c)) \tag{35}$$

The right-hand side of (35) can be written as

$$\begin{aligned}
&\mathcal{J}^{\text{P}}(\underline{x}^{\text{P}}(k_c+j))-V(\underline{x}^{\text{C}}(k_c|k_c))\\
&=\sum_{h=K_p}^{K_p+j-1}\sum_{i=1}^{N}\gamma_i^{\rho}\tilde{\rho}_i^{\text{P}}(k_c+h)+\gamma_i^{l}\tilde{l}_i^{\text{P}}(k_c+h)+\gamma_i^{\varrho}\tilde{\varrho}_i^{\text{P}}(k_c+h)\\
&\quad+\sum_{h=j}^{K_p-1}\sum_{i=1}^{N}\gamma_i^{\rho}\left(\rho_i^{\text{P}}(k_c+h)-\rho_i^{\text{C}}(k_c+h|k_c)\right)+\gamma_i^{l}\left(l_i^{\text{P}}(k_c+h)-l_i^{\text{C}}(k_c+h|k_c)\right)\\
&\quad+\sum_{h=j}^{K_p-1}\sum_{i=1}^{N}\gamma_i^{\varrho}\left(\varrho_i^{\text{P}}(k_c+h)-\varrho_i^{\text{C}}(k_c+h|k_c)\right)\\
&\quad-\sum_{h=0}^{j-1}\sum_{i=1}^{N}\gamma_i^{\rho}\rho_i^{\text{C}}(k_c+h|k_c)+\gamma_i^{l}l_i^{\text{C}}(k_c+h|k_c)+\gamma_i^{\varrho}\varrho_i^{\text{C}}(k_c+h|k_c)
\end{aligned} \tag{36}$$

Thanks to Proposition 1, it is

$$\begin{aligned}
&\mathcal{J}^{\text{P}}(\underline{x}^{\text{P}}(k_c+j))-V(\underline{x}^{\text{C}}(k_c|k_c))\\
&\leqslant\sum_{h=K_p}^{K_p+j-1}\sum_{i=1}^{N}\gamma_i^{\rho}\tilde{\rho}_i^{\text{P}}(k_c+h)+\gamma_i^{l}\tilde{l}_i^{\text{P}}(k_c+h)+\gamma_i^{\varrho}\tilde{\varrho}_i^{\text{P}}(k_c+h)\\
&\quad+(K_p-j)\sum_{i=1}^{N}\left(\gamma_i^{\rho}\epsilon_i^{\rho}+\gamma_i^{l}\epsilon_i^{l}\right)+\sum_{h=j}^{K_p-1}\sum_{i=1}^{N}\gamma_i^{\rho}\kappa_i^{\rho}(k_c+h)\Omega_i^{\rho}+\gamma_i^{l}\kappa_i^{l}(k_c+h)\Omega_i^{l}\\
&\quad+\sum_{h=j}^{K_p-1}\sum_{i=1}^{N}\gamma_i^{\varrho}\left(\varrho_i^{\text{P}}(k_c+h)-\varrho_i^{\text{C}}(k_c+h|k_c)\right)\\
&\quad-\sum_{h=0}^{j-1}\sum_{i=1}^{N}\gamma_i^{\rho}\rho_i^{\text{C}}(k_c+h|k_c)+\gamma_i^{l}l_i^{\text{C}}(k_c+h|k_c)+\gamma_i^{\varrho}\varrho_i^{\text{C}}(k_c+h|k_c)
\end{aligned} \tag{37}$$

By considering that the system state is limited in the present case, one has

$$\begin{aligned}
&\mathcal{J}^{\text{P}}(\underline{x}^{\text{P}}(k_c+j))-V(\underline{x}^{\text{C}}(k_c|k_c))\\
&\leqslant j\sum_{i=1}^{N}\left(\gamma_i^{\rho}+\gamma_i^{\varrho}\right)\bar{\rho}_i+\gamma_i^{l}\bar{l}_i\\
&\quad+(K_p-j)\sum_{i=1}^{N}\left(\gamma_i^{\rho}\epsilon_i^{\rho}+\gamma_i^{l}\epsilon_i^{l}\right)+\sum_{h=j}^{K_p-1}\sum_{i=1}^{N}\gamma_i^{\rho}\kappa_i^{\rho}(k_c+h)\Omega_i^{\rho}+\gamma_i^{l}\kappa_i^{l}(k_c+h)\Omega_i^{l}\\
&\quad+\sum_{h=j}^{K_p-1}\sum_{i=1}^{N}\gamma_i^{\varrho}\bar{\rho}_i-\sum_{i=1}^{N}\gamma_i^{\min}\left(\rho_i^{\text{C}}(k_c|k_c)+l_i^{\text{C}}(k_c|k_c)\right)
\end{aligned} \tag{38}$$

DOI: 10.1002/rnc

It follows that

$$V(\underline{x}^{\mathrm{C}}(k_c+j|k_c+j))-V(\underline{x}^{\mathrm{C}}(k_c|k_c)) \leqslant -\gamma^{\min}\sum_{i=1}^{N}\left|\rho_i^{\mathrm{C}}(k_c|k_c)\right|+\left|l_i^{\mathrm{C}}(k_c|k_c)\right| + \sum_{h=j}^{K_p-1}\sum_{i=1}^{N}\gamma_i^{\rho}\kappa_i^{\rho}(k_c+h)\Omega_i^{\rho}+\gamma_i^{l}\kappa_i^{l}(k_c+h)\Omega_i^{l}+c_2 \tag{39}$$

which, c_2 being a constant term, proves (34). □

Thanks to Lemmas 1 and 2, by exploiting Lemma 3.5 in [19], it can be concluded that condition (23) is verified for all time steps $k_c \in \Upsilon$. It is now possible to prove the ISpS for the freeway traffic system controlled via the proposed event-triggered control scheme.

Theorem 1

The freeway traffic control system subject to the application of the proposed control scheme is ISpS for initial conditions in X_0 and exogenous inputs in W.

Proof

In order to prove this theorem, it is necessary to verify condition (23) for all time steps $k = 1,\ldots,K$ (by following the same reasoning line proposed in the proof of Theorem 1 in [27]). As aforementioned, Lemmas 1 and 2, by exploiting Lemma 3.5 in [19], guarantee that condition (23) is verified for all the triggering time steps $k_c \in \Upsilon$. It is now necessary to prove the same condition for time steps that are not triggering time steps, that is, for $k \notin \Upsilon$. The following holds:

$$\begin{aligned} V(\underline{x}^{\mathrm{C}}(k_c|k_c)) &= \sum_{h=k_c}^{k_c+K_p-1}\sum_{i=1}^{N}\gamma_i^{\rho}\rho_i^{\mathrm{C}}(h|k_c)+\gamma_i^{l}l_i^{\mathrm{C}}(h|k_c)+\gamma_i^{\varrho}\varrho_i^{\mathrm{C}}(h|k_c) \\ &\geqslant \gamma^{\min}\sum_{h=k_c}^{k_c+K_p-1}\sum_{i=1}^{N}\left|\rho_i^{\mathrm{C}}(h|k_c)\right|+\left|l_i^{\mathrm{C}}(h|k_c)\right| \end{aligned} \tag{40}$$

Moreover, from Proposition 1, it can be derived that

$$\begin{aligned} &|\rho_i^{\mathrm{P}}(h)|-\left|\rho_i^{\mathrm{C}}(h|k_c)\right| \leqslant \epsilon_i^{\rho}+\kappa_i^{\rho}(h)\cdot\Omega_i^{\rho} \qquad i=1,\ldots,N,\ k=k_c+1,\ldots,k_c+K_p-1 \\ &|l_i^{\mathrm{P}}(h)|-\left|l_i^{\mathrm{C}}(h|k_c)\right| \leqslant \epsilon_i^{l}+\kappa_i^{l}(h)\cdot\Omega_i^{l} \qquad i=1,\ldots,N,\ k=k_c+1,\ldots,k_c+K_p-1 \end{aligned} \tag{41}$$

By substituting (41) in (40), one has

$$V(\underline{x}^{\mathrm{C}}(k_c|k_c)) \geqslant \gamma^{\min}\sum_{h=k_c}^{k_c+K_p-1}\sum_{i=1}^{N}\left[|\rho_i^{\mathrm{P}}(h)|+|l_i^{\mathrm{P}}(h)|-\epsilon_i^{\rho}-\kappa_i^{\rho}(h)\cdot\Omega_i^{\rho}-\epsilon_i^{l}-\kappa_i^{l}(h)\cdot\Omega_i^{l}\right] \tag{42}$$

Because $k_c < k < k_c+K_p-1$, (42) gives

$$\begin{aligned} \sum_{i=1}^{N}|\rho_i^{\mathrm{P}}(k)|+|l_i^{\mathrm{P}}(k)| &\leqslant \sum_{h=k_c}^{k_c+K_p-1}\sum_{i=1}^{N}|\rho_i^{\mathrm{P}}(h)|+|l_i^{\mathrm{P}}(h)| \leqslant \frac{1}{\gamma^{\min}}V(\underline{x}^{\mathrm{C}}(k_c|k_c)) \\ &+\sum_{h=k_c}^{k_c+K_p-1}\sum_{i=1}^{N}\left[\epsilon_i^{\rho}+\kappa_i^{\rho}(h)\cdot\Omega_i^{\rho}+\epsilon_i^{l}+\kappa_i^{l}(h)\cdot\Omega_i^{l}\right] \end{aligned} \tag{43}$$

Because condition (23) is verified for all time steps $k_c \in \Upsilon$, it is possible to find a $\mathcal{KL}$ function $\tilde{\beta}(\cdot,\cdot)$, a $\mathcal{K}$-function $\tilde{\gamma}(\cdot)$, and a non-negative constant $\tilde{c}$ such that

$$V(\|\underline{x}^{\mathrm{C}}(k_c|k_c)\|) \leqslant \tilde{\beta}(V(\|\underline{x}(0)\|),k_c)+\tilde{\gamma}(\Omega)+\tilde{c} \tag{44}$$

DOI: 10.1002/rnc

Moreover, it holds

$$\begin{aligned} V(\|\underline{x}^{\mathrm{C}}(k_c|k_c)\|) &= \sum_{h=k_c}^{k_c+K_p-1}\sum_{i=1}^{N}\gamma_i^{\rho}\rho_i^{\mathrm{C}}(h|k_c)+\gamma_i^{l}l_i^{\mathrm{C}}(h|k_c)+\gamma_i^{\varrho}\varrho_i^{\mathrm{C}}(k_c+h|k_c) \\ &\leqslant \gamma^{\max}\sum_{i=1}^{N}\left|\rho_i^{\mathrm{C}}(k_c|k_c)\right|+\left|l_i^{\mathrm{C}}(k_c|k_c)\right| \\ &\quad +\gamma^{\max}(K_p-1)\sum_{i=1}^{N}\left(\bar{\rho}_i+\bar{l}_i\right)=\psi_1\|\underline{x}^{\mathrm{C}}(k_c|k_c)\|+\psi_2 \end{aligned} \tag{45}$$

where ψ_1 and ψ_2 are constant terms and the one-norm is considered. Then, taking into account (44) and (45), the following holds:

$$V(\|\underline{x}^{\mathrm{C}}(k_c|k_c)\|)\leqslant\tilde{\beta}(\psi_1\|\underline{x}(0)\|+\psi_2,k_c)+\tilde{\gamma}(\Omega)+\tilde{c} \tag{46}$$

By substituting (46) in (43), it is possible to find a $\mathcal{KL}$ function $\beta(\cdot,\cdot)$, a $\mathcal{K}$-function $\gamma(\cdot)$, and a non-negative constant c such that condition (23) is verified also for $k\notin\Upsilon$, which concludes the proof. □

6. SIMULATION RESULTS

The proposed control framework has been implemented with the C Sharp (C♯) programming language, and the finite-horizon optimal control problems have been solved via the mixed-integer linear programming solver IBM ILOG Cplex 12.5. The objective of the simulation campaign is, first of all, to compare the performance of the freeway system controlled via the proposed control scheme with the case of an uncontrolled freeway system and the case of a freeway system controlled via a standard MPC (in which at each time step, the state is transmitted and the finite-horizon optimal control problem is solved). Moreover, in this section, we will show how the performance of the proposed controller varies depending on the amplitude of the disturbances and on the choice of the triggering threshold values.

The controller predictor is the CTM in MLD form, whereas the dynamic model adopted by the emulator and used to represent the dynamic evolution of the plant is the CTM. To take into account the model inaccuracy of the controller predictor compared with the emulator, as well as the model inaccuracy of the emulator compared with the plant, random terms have been added to the system state variables. Moreover, both the controller predictor and the emulator do not know precisely the real demands at the on-ramps and in the cell before the first one, and then, they simply use an estimation of such demands determined, for instance, on the basis of historical data.

As aforementioned, the proposed control scheme will be compared with the no-control case and with a standard MPC framework. To make such a comparison, the evolution of the state variables will be considered, as well as three performance indexes. First, the control objective (7) is computed over the entire time horizon K, that is, $J=\sum_{k=1}^{K}\sum_{i=1}^{N}\gamma_i^{\rho}\rho_i(k)+\gamma_i^{l}l_i(k)+\gamma_i^{\varrho}\varrho_i(k)$ for the three cases. Then, for the two controlled systems (with standard MPC and event-triggered MPC), the *objective percentage difference* ΔJ compared with the no-control case is computed (a negative ΔJ means that the controlled system has reduced the control objective J compared with the no-control case).

In addition, because the proposed control scheme has been designed to reduce the number of computations by the controller and the number of state transmissions from the sensors to the controller, the second and third performance indexes are related to computations and transmissions. Specifically, the second index is the *computation ratio*, denoted with $\mathcal{C}$ and defined as $\mathcal{C}=\frac{1}{K}\sum_{k=1}^{K}c(k)$, where $c(k)$ is equal to 1 if the finite-horizon optimal control problem is solved at time step k, while it is equal to 0 otherwise. Analogously, a *transmission ratio* is considered, denoted with $\mathcal{T}$, and defined as $\mathcal{T}=\frac{1}{KN}\sum_{k=1}^{K}\sum_{i=1}^{N}t_i(k)$, where $t_i(k)$ is equal to 1 if a measurement is transmitted from the sensor in cell i at time step k, while it is equal to 0 otherwise. Then, when the standard

DOI: 10.1002/rnc

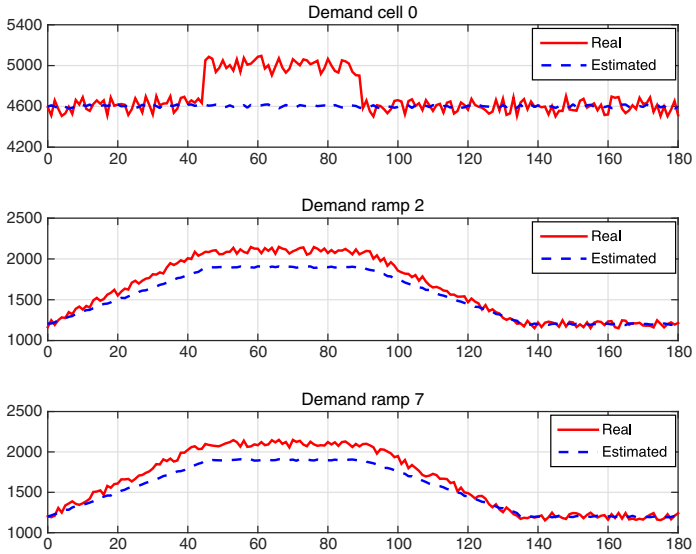

Figure 3. Scenario 1: real and estimated demands.

MPC is applied, it is $\mathcal{C} = 1$ and $\mathcal{T} = 1$ by definition, whereas it is $\mathcal{C} \leqslant 1$ and $\mathcal{T} \leqslant 1$ for the event-triggered MPC scheme.

Four scenarios will be analyzed, starting from a basic one (scenario 1), whereas scenarios 2, 3, and 4 differ from scenario 1 for the demand estimation or the amplitude of the errors among the different models. Finally, a specific analysis will be devoted to show the event-triggered control scheme behavior when the triggering threshold values change.

6.1. Scenario 1: basic case

The considered freeway stretch is composed of 12 cells with two ramps (in cells 2 and 7). The cells are characterized by $L_i = 0.7\,[\text{km}]$, $v_i = 100\,[\text{km/h}]$, $w_i = 35\,[\text{km/h}]$, $F_i = 8000\,[\text{veh/h}]$, $\bar{\rho}_i = 450\,[\text{veh/km}]$, $i = 1, \ldots, 12$. The ramp parameters are $\beta_{i-1} = 0.05$ and $p_i = 0.4$, $i = 2, 7$. The initial traffic density has been set equal to 80 [veh/km] in all the cells, whereas the initial queue lengths are equal to 0 in the two on-ramps. The simulation covers 1 h, corresponding to $K = 180$ (adopting a sample time $T = 20\,[\text{s}]$).

The parameters of the event-triggered controller are the following: $K_p = 12$, $\rho_i^{\text{t}} = 90\,[\text{veh/km}]$, $\gamma_i^{\rho} = \gamma_i^{l} = 1$, $\gamma_i^{\varrho} = 0.01$, $\bar{r}_i = 3000\,[\text{veh/h}]$, $\epsilon_i^{\rho} = 5$, $\epsilon_i^{l} = 10$, $\kappa_i^{\rho}(k)\Omega_i^{\rho} = 5$, and $\kappa_i^{l}(k)\Omega_i^{l} = 10$, $\forall k$, $i = 1, \ldots, 12$. The random terms added to model the inaccuracy of the controller predictor compared with the emulator have been generated from the uniform distribution and range between -2.5 and 2.5 for the density and between -0.5 and 0.5 for the queues. Analogously, to reproduce the inaccuracy of the emulator compared with the plant (which is lower than the inaccuracy of the predictor compared with the emulator), random terms have been generated from the uniform distribution, ranging between -1 and 1 for the density and between -0.5 and 0.5 for the queues. In this scenario, both the demand from cell 0 and the on-ramp demands are underestimated by the emulators and the predictor, as shown in Figure 3.

The evolution of the traffic density in each cell over the entire time horizon is depicted in Figure 4, for the no-control case, the case in which a standard MPC is applied and the case in which the proposed event-triggered control scheme is used. Analogously, Figure 5 reports the queue lengths in the three cases. Analyzing Figures 4 and 5, we have observed that the no-control case is characterized by very high values of the density in cells 5 and 6, whereas in the two controlled cases such a congestion is reduced, thanks to the ramp metering action, which, on the other hand, induces the formation of some queues. Figure 6 reports the control input in the two controlled cases.

These controlled cases are characterized respectively by the following performance indexes:

- standard MPC: $\Delta J = -0.39$, $\mathcal{C} = 1$, $\mathcal{T} = 1$;

DOI: 10.1002/rnc

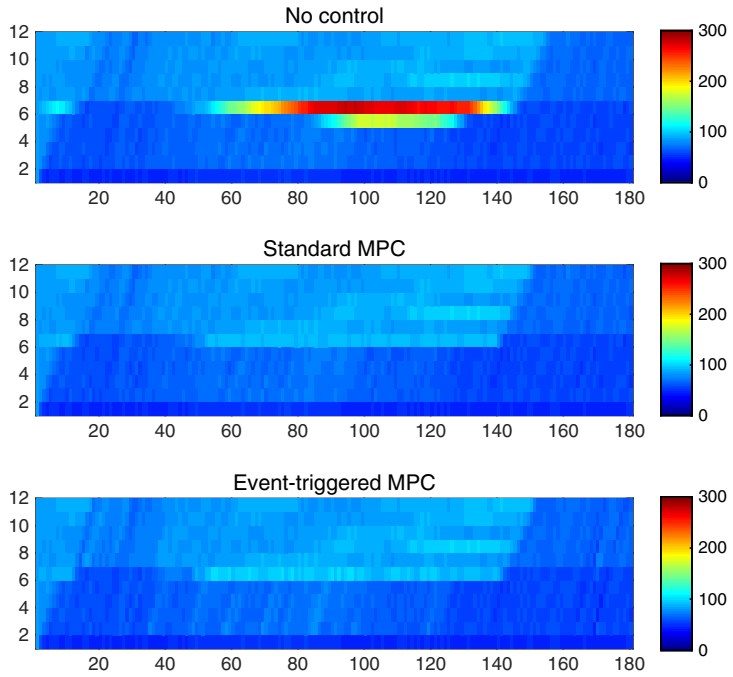

Figure 4. Scenario 1: density evolution.

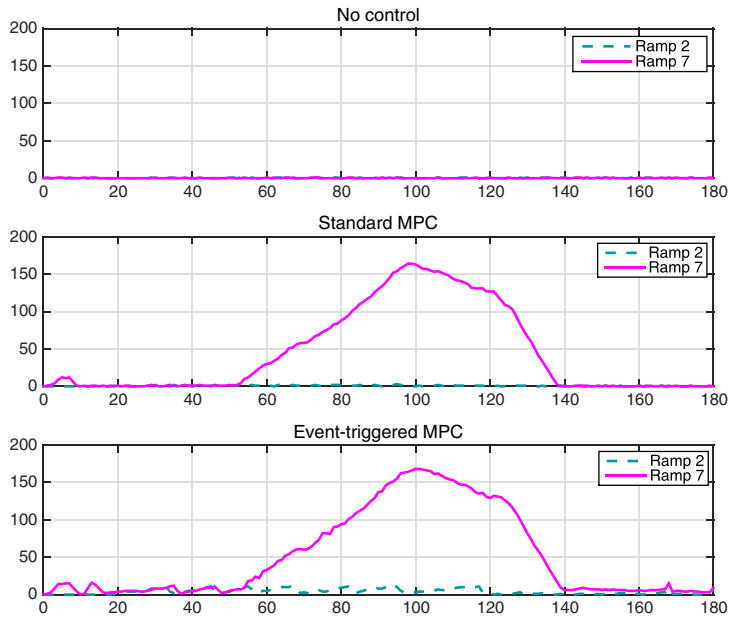

Figure 5. Scenario 1: queues evolution.

- event-triggered MPC: $\Delta J = -0.28, \mathcal{C} = 0.31, \mathcal{T} = 0.017$.

Hence, the event-triggered MPC shows a good performance in terms of cost reduction (28% reduction of the cost function with respect to the no-control case) by highly reducing the number of computations (55 instead of 180) and the number of transmissions (36 instead of 2160) if compared with a standard MPC controller.

Figures 7 and 8 report the evolution in time of the density errors, respectively, between the plant and the emulator and between the emulator and the predictor. Both the errors range between -5 and

DOI: 10.1002/rnc

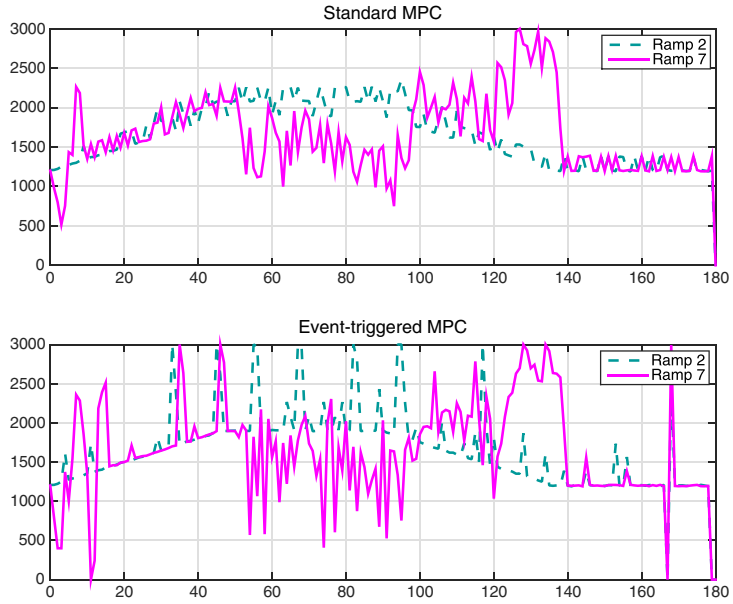

Figure 6. Scenario 1: control input evolution.

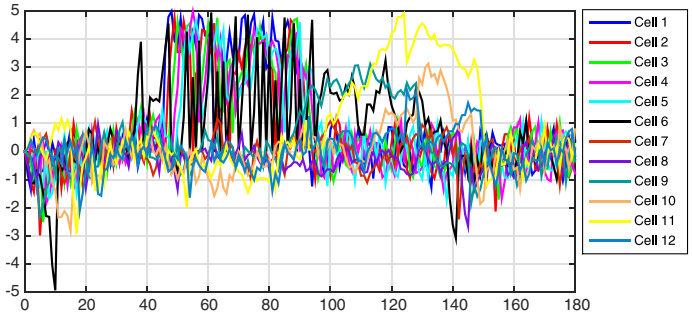

Figure 7. Scenario 1: density error between the plant and the emulator.

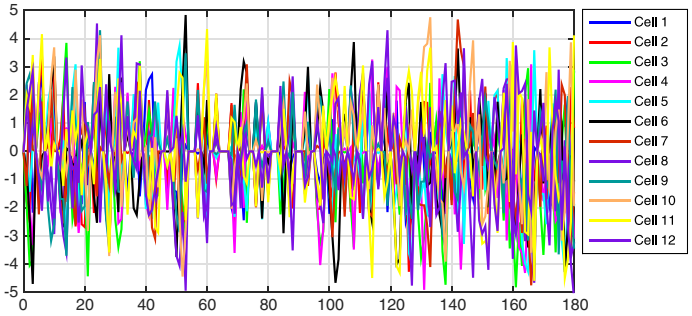

Figure 8. Scenario 1: density error between the emulator and the predictor.

5 because these are the threshold values chosen for the density. Note that the error between the plant and the emulator (Figure 7) is positive between time steps 40 and 90, when the real density is higher than the one computed by the emulator because the demands have been underestimated. On the contrary, the difference between the density computed by the emulator and the one provided by the predictor (Figure 8) seems to have zero mean because such difference is only due to the inaccuracy that we have modeled as a uniformly distributed random term (ranging between -2.5 and 2.5).

DOI: 10.1002/rnc

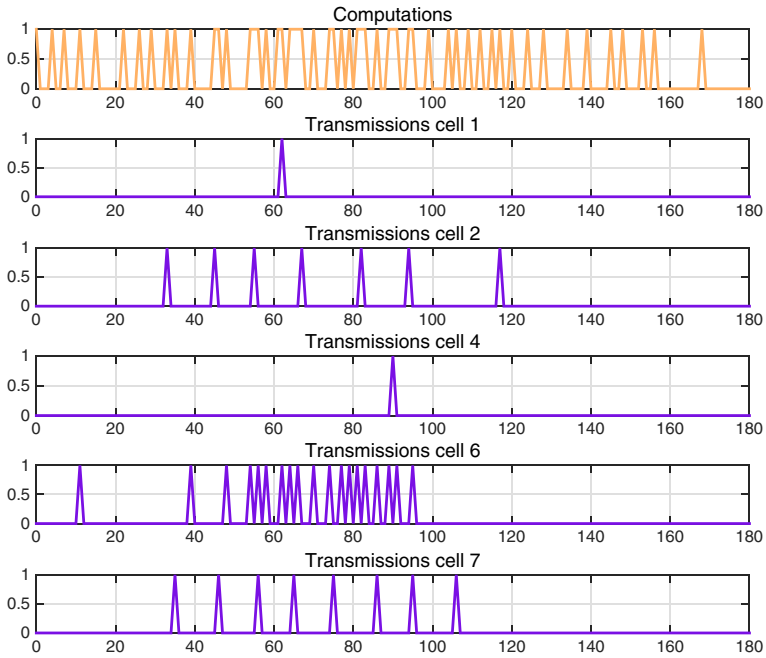

Figure 9. Scenario 1: computations and transmissions.

Figure 9 shows in which time steps the finite-horizon problem has been computed and in which time steps the cells have transmitted the measured state (the cells that have never transmitted their state are not reported). More specifically, the curves in Figure 9 are binary signals equal to 1 when a computation or a transmission is realized. It is worth highlighting that most of the transmissions are realized between time steps 40 and 120, that is, when the error of the estimated demand is higher. For the same reason, only cells 1, 2, 4, 6, and 7 transmit their state because they are more involved by this estimation error (which affects cell 0, and cells 2 and 7 that are equipped with on-ramps).

Finally, let us report some indications about computational issues, taking into account that all the experimental tests have been realized with a computer with a 3-GHz Intel Core i7 processor and 16-GB RAM. The finite-horizon optimal control problem to be solved at each time step is characterized by 1848 variables and 4162 constraints. When the standard MPC is applied, the average computational time to solve each finite-horizon optimal control problem is 0.19 [s], and the maximum time is 1.01 [s]. Similar computational times characterize the case in which the event-triggered MPC controller is adopted (average computational time of 0.19 [s] and maximum computational time of 1.03 [s]).

6.2. Scenario 2: overestimation of the demands

Scenario 2 is characterized by the same parameters of scenario 1, except for the estimation of the demands. In this scenario, the emulator and the predictors overestimate the demand from cell 0 and the on-ramp demands, as shown in Figure 10. The performance indexes of the controlled cases in scenario 2 are very similar to scenario 1 and present the following values:

- standard MPC: $\Delta J = -0.35, \mathcal{C} = 1, \mathcal{T} = 1$;
- event-triggered MPC: $\Delta J = -0.32, \mathcal{C} = 0.33, \mathcal{T} = 0.025$.

Again, the event-triggered MPC scheme guarantees a very good performance of the controlled freeway system by strongly limiting the number of computations and state transmissions. Also the behaviors of the state variables are very similar to scenario 1 and are not reported here for brevity. The error between the density computed by the emulator and the density computed by the predictor is very similar to the one shown in Figure 8, whereas the density error between the plant and the emulator is shown in Figure 11. By comparing Figure 11 with Figure 7, it can be seen that such an

DOI: 10.1002/rnc

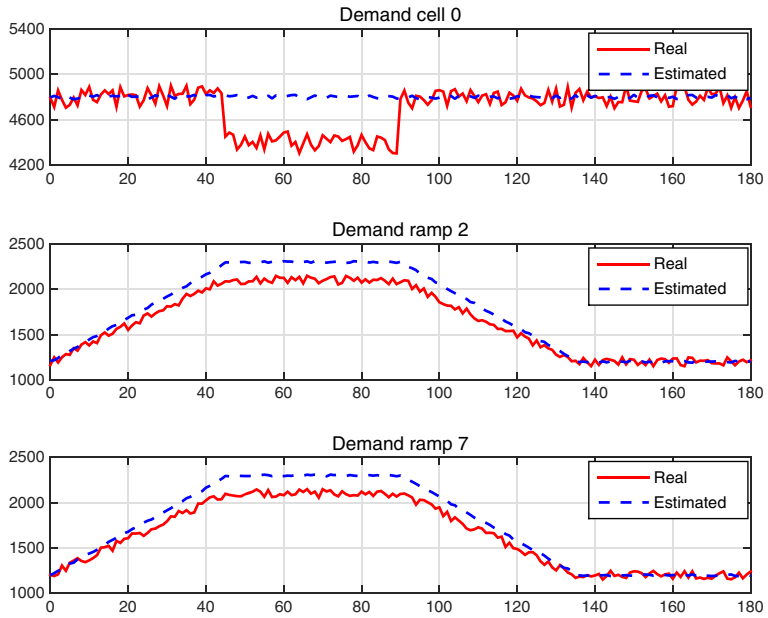

Figure 10. Scenario 2: real and estimated demands.

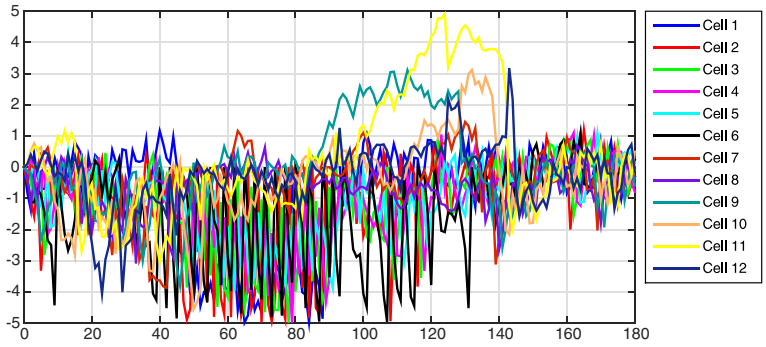

Figure 11. Scenario 2: density error between the plant and the emulator.

error is negative in scenario 2 in the same time period (between time steps 40 and 90) in which it is positive in scenario 1. This is obviously due to the overestimation of the demand.

As for the transmissions from the sensors to the controller (53 in this scenario), they are carried out by cells 1, 2, 3, 5, 6, 7, and 11, mainly between time steps 40 and 120, because in this period, the estimation error is higher. In summary, the performances of the controlled freeway in scenario 2 are very similar to those in scenario 1. This means that the characteristics of the control scheme are not influenced by the fact that the demand is overestimated or underestimated, because they are instead mainly influenced by the error amplitude.

6.3. Scenario 3: stronger underestimation

Scenario 3 is obtained from scenario 1 but considering a higher estimation error. Specifically, as shown in Figure 12, the demands are again underestimated.

The performance indexes of the controlled cases present the following values:

- standard MPC: $\Delta J = -0.37, \mathcal{C} = 1, \mathcal{T} = 1$;
- event-triggered MPC: $\Delta J = -0.28, \mathcal{C} = 0.38, \mathcal{T} = 0.033$.

Because the estimation error is higher than in scenario 1 and having maintained the same threshold values, the number of computations and transmissions is increased with respect to scenario 1. In

DOI: 10.1002/rnc

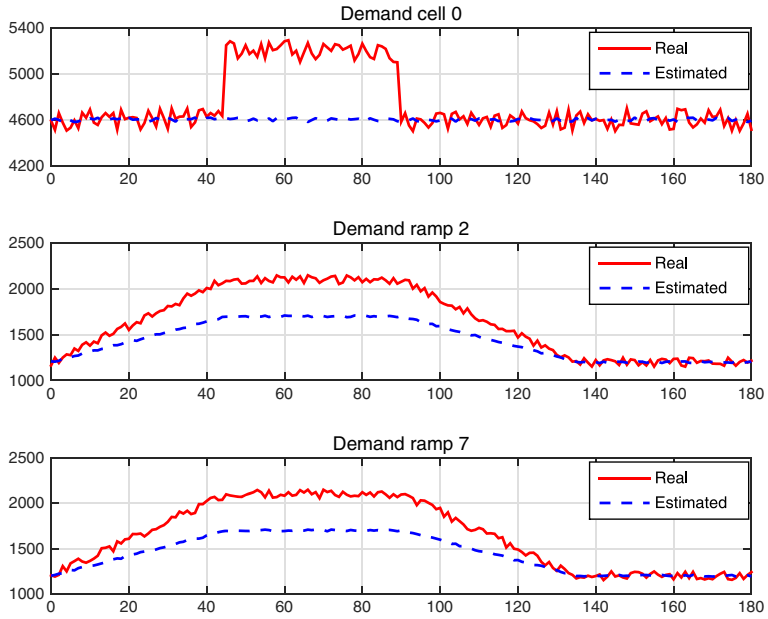

Figure 12. Scenario 3: real and estimated demands.

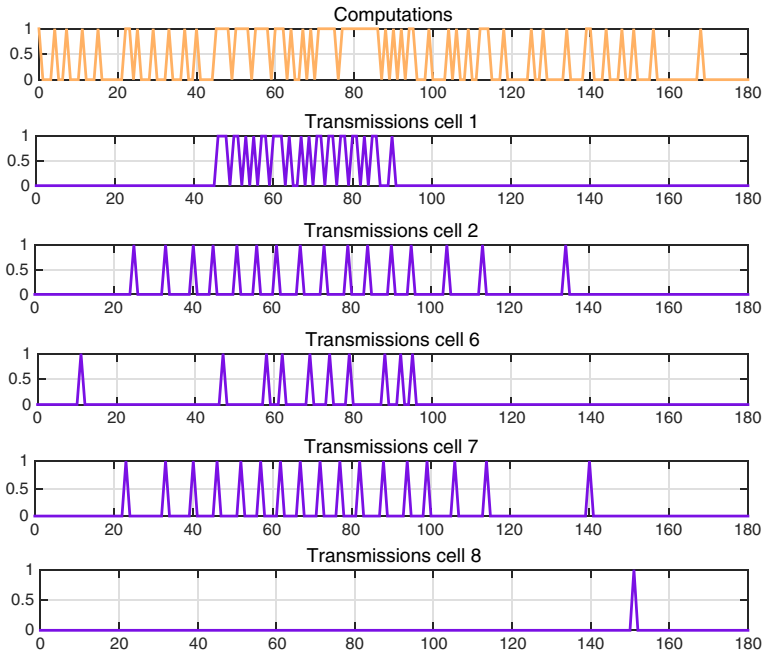

Figure 13. Scenario 3: computations and transmissions.

particular, Figure 13 shows the computations and transmissions over the considered time horizon. Between time steps 40 and 90, the control problem is almost solved at each time step, and the cells that transmit their state are again those more affected by the estimation error (cells 1, 2, 6, 7, and 8).

6.4. Scenario 4: higher error of the predictor compared with the emulator

Scenario 4 is obtained from scenario 1 by considering a less accurate predictor. Indeed, in scenario 4, the random terms added to model the inaccuracy of the controller predictor compared with the

DOI: 10.1002/rnc

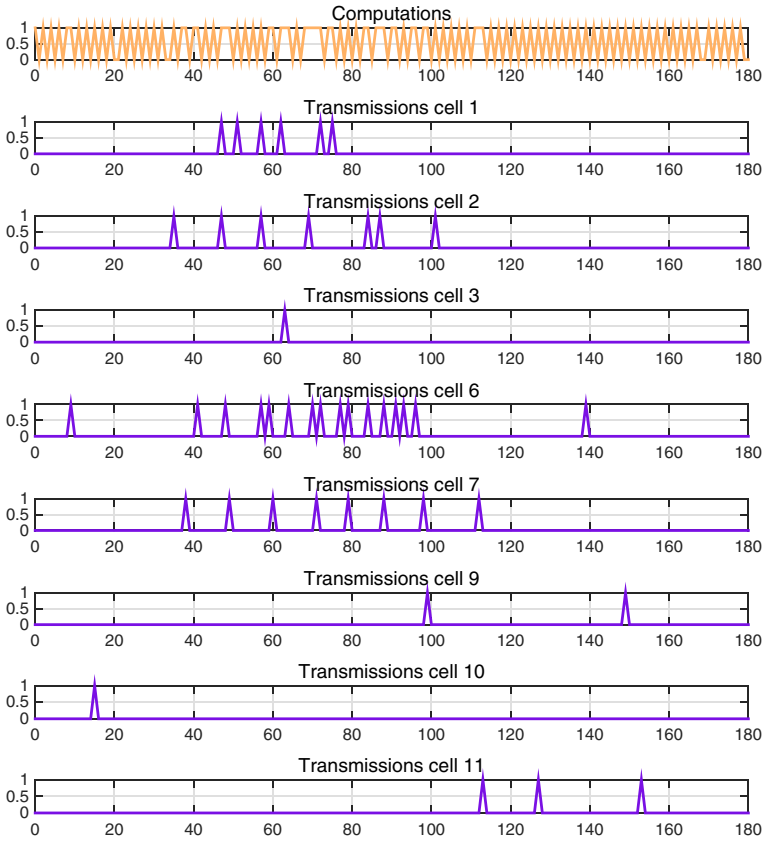

Figure 14. Scenario 4: computations and transmissions.

emulator range between -5 and 5 for the density and between -1 and 1 for the queues. The two controlled cases are characterized by:

- standard MPC: $\Delta J = -0.34, \mathcal{C} = 1, \mathcal{T} = 1$;
- event-triggered MPC: $\Delta J = -0.22, \mathcal{C} = 0.55, \mathcal{T} = 0.020$.

Comparing these indexes with those of scenario 1, we have seen that the number of computations is doubled, and this is motivated by a less accurate predictor, which activates more frequently the controller triggering condition. Figure 14 reports in detail the computation and transmission signal.

6.5. *Change of the threshold values*

A final simulation analysis regards the different behaviors of the event-triggered control scheme with different threshold values used in the triggering conditions of the sensors and the controller. In particular, scenario 1 is considered with different sets of threshold values, corresponding to the following seven cases (case 1 corresponds to the strictest triggering conditions):

1. $\epsilon_i^\rho = \kappa_i^\rho(k)\Omega_i^\rho = 1, \epsilon_i^l = \kappa_i^l(k)\Omega_i^l = 2, \forall k, \forall i$;
2. $\epsilon_i^\rho = \kappa_i^\rho(k)\Omega_i^\rho = 2, \epsilon_i^l = \kappa_i^l(k)\Omega_i^l = 5, \forall k, \forall i$;
3. $\epsilon_i^\rho = \kappa_i^\rho(k)\Omega_i^\rho = 5, \epsilon_i^l = \kappa_i^l(k)\Omega_i^l = 10, \forall k, \forall i$;
4. $\epsilon_i^\rho = \kappa_i^\rho(k)\Omega_i^\rho = 8, \epsilon_i^l = \kappa_i^l(k)\Omega_i^l = 15, \forall k, \forall i$;
5. $\epsilon_i^\rho = \kappa_i^\rho(k)\Omega_i^\rho = 10, \epsilon_i^l = \kappa_i^l(k)\Omega_i^l = 20, \forall k, \forall i$;
6. $\epsilon_i^\rho = \kappa_i^\rho(k)\Omega_i^\rho = 12, \epsilon_i^l = \kappa_i^l(k)\Omega_i^l = 25, \forall k, \forall i$;
7. $\epsilon_i^\rho = \kappa_i^\rho(k)\Omega_i^\rho = 15, \epsilon_i^l = \kappa_i^l(k)\Omega_i^l = 30, \forall k, \forall i$;

Figure 15 reports the three performance indexes of the event-triggered MPC scheme in the seven cases listed before. As expected, when the triggering conditions become less strict (i.e., the threshold

DOI: 10.1002/rnc

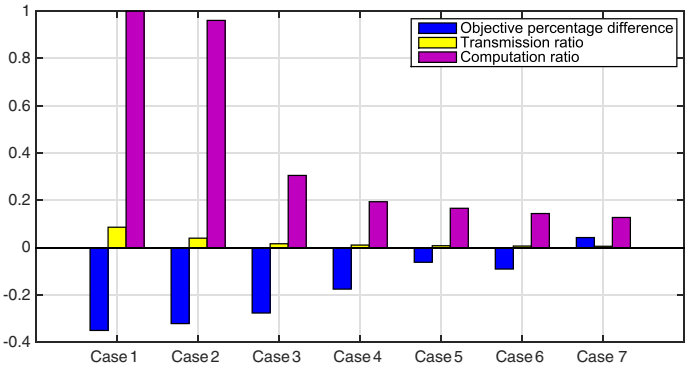

Figure 15. Performance indexes ΔJ, $\mathcal{T}$, and $\mathcal{C}$ depending on the threshold values.

values increase, from case 1 to case 7), the performance improvement of the controlled system compared with the no-control case is reduced (in case 1, $\Delta J = -0.35$ indicates that there is a 35% reduction of the control objective, while in case 7, $\Delta J = 0.04$ means that the controlled system performs even slightly worse than the no-control one). At the same time, higher threshold values correspond to a lower number of computations and transmissions (from case 1 to case 7, the transmission ratio $\mathcal{T}$ varies between 0.087 and 0.006 and the computation ratio $\mathcal{C}$ ranges between 1 and 0.13). It can be then concluded that by increasing the threshold values, the event-triggered MPC scheme shows a performance deterioration, but this 'cost' is counterbalanced by the 'benefit' of significantly decreasing the number of computations and transmissions.

7. CONCLUSIONS

An MPC networked scheme for freeway traffic systems has been designed in this paper. The main aim of the proposed scheme is that of limiting the computational and communication effort in order to increase its practical applicability. As for the computational load, suitable event-triggered logics are included in the plant controller in order to compute the control action only when it is actually convenient. The same has been carried out in the sensor structure for which triggering conditions are defined to verify when it is necessary to transmit the measured state. The ISpS of the controlled system has been proved. In addition, simulation results have shown that the proposed framework can actually constitute a suitable way to keep the computational burden and communication effort low, without significantly decreasing the performance of the controlled system with respect to those obtained via a standard MPC.

REFERENCES

1. Papageorgiou M, Kotsialos A. Freeway ramp metering: an overview. *IEEE Transactions on Intelligent Transportation Systems* 2002; **3**:271–281.
2. Papageorgiou M, Papamichail I. Overview of traffic signal operation policies for ramp metering. *Transportation Research Record: Journal of the Transportation Research Board* 2008; **2047**:28–36.
3. Papageorgiou M, Hadj-Salem H, Blosseville J-M. ALINEA: a local feedback control law for on-ramp metering. *Transportation Research Record* 1991; **1320**:58–64.
4. Kotsialos A, Papageorgiou M. Motorway network traffic control systems. *European Journal of Operational Research* 2004; **152**:321–333.
5. Kotsialos A, Papageorgiou M, Middelham F. Optimal coordinated ramp metering with AMOC. *Transportation Research Record* 2001; **1748**:55–65.
6. Papageorgiou M, Kotsialos A. Nonlinear optimal control applied to coordinated ramp metering. *IEEE Transactions on Intelligent Transportation Systems* 2004; **12**:920–933.
7. Hegyi A, De Schutter B, Hellendoorn H. Model predictive control for optimal coordination of ramp metering and variable speed limits. *Transportation Research C* 2005; **13**:185–209.
8. Bellemans T, De Schutter B, De Moor B. Model predictive control for ramp metering of motorway traffic: a case study. *Control Engineering Practice* 2006; **14**:757–767.

DOI: 10.1002/rnc

9. Papageorgiou M, Blosseville JM, Hadj-Salem H. Modelling and realtime control of traffic flow on the southern part of Boulevard Périphérique in Paris: Part I: Modelling. *Transportation Research A* 1990; **24**:345–359.
10. Ferrara A, Nai Oleari A, Sacone S, Siri S. An event-triggered model predictive control scheme for freeway systems, 2012; 6975–6982.
11. Ferrara A, Sacone S, Siri S. Event-triggered model predictive schemes for freeway traffic control. *Transportation Research C* Available online 21 February 2015. DOI: 10.1016/j.trc.2015.01.020.
12. Daganzo CF. The cell transmission model: a dynamic representation of highway traffic consistent with the hydrodynamic theory. *Transportation Research Part B* 1994; **28**:269–287.
13. Daganzo CF. The cell transmission model, part II: network traffic. *Transportation Research Part B* 1995; **29**:79–93.
14. Bemporad A, Morari M. Control of systems integrating logic, dynamics, and constraints. *Automatica* 1999; **35**: 407–427.
15. Hespanha JP, Naghshtabrizi P, Xu Y. A survey of recent results in networked control system. *Proceedings of the IEEE* 2007; **95**:138–162.
16. Gupta RA, Chow M-Y. Networked control system: overview and research trends. *IEEE Transactions on Industrial Electronics* 2010; **57**:2527–2535.
17. Liu S, Frejo JRD, Nunez A, De Schutter B, Sadowska A, Hellendoorn H, Camacho EF. Tractable robust predictive control approaches for freeway networks, 2014; 1857–1862.
18. Sontag ED, Wang Y. New characterizations of input-to-state stability. *IEEE Transactions on Automatic Control* 1996; **41**:1283–1294.
19. Jiang ZP, Wang Y. Input-to-state stability for discrete-time nonlinear systems. *Automatica* 2001; **37**:857–869.
20. Sontag ED. Input to state stability: basic concepts and results. In *Nonlinear and Optimal Control Theory*, 2008; 163–220.
21. Bianchi D, Ferrara A, Di Benedetto MD. Networked model predictive traffic control with time varying optimization horizon: the Grenoble South Ring case study. *Proceedings of the European Control Conference*, Zurich, Switzerland, 2013; 4039–4044.
22. Nagel K, Shreckenberg M. A cellular automaton model for freeway traffic. *Journal de Physique I* 1992; **2**:2221–2229.
23. Barceló J. *Fundamentals in Traffic Simulation*. Springer: New York, 2010.
24. Ferrara A, Sacone S, Siri S. Event-triggered strategies for the networked control of freeway traffic systems, 2014; 2594–2599.
25. Lazar M, Heemels WPMH. Predictive control of hybrid systems: input-to-state stability results for sub-optimal solutions. *Automatica* 2009; **45**:180–185.
26. Limon D, Alamo T, Raimondo DM, Muñoz de la Peña D, Bravo JM, Ferramosca A, Camacho EF. Input-to-state stability: a unifying framework for robust model predictive control. In *Nonlinear Model Predictive Control*, Magni, L. *et al.* (ed.). Springer-Verlag: Berlin Heidelberg, 2009; 1–26.
27. Quevedo DE, Nešić D. Input-to-state stability of packetized predictive control over unreliable networks affected by packet-dropouts. *IEEE Transactions on Automatic Control* 2011; **56**:370–375.

DOI: 10.1002/rnc